Optics Letters

Nanosecond pulsed 620 nm source by frequency-doubling a phosphosilicate Raman fiber amplifier

A. M. Chandran,* T. H. Runcorn, R. T. Murray, and J. R. Taylor

Femtosecond Optics Group, Department of Physics, Imperial College London, Prince Consort Road, London, SW7 2BW, UK
**Corresponding author: anita.chandran13@imperial.ac.uk*

Received 25 October 2019; accepted 4 November 2019; posted 12 November 2019 (Doc. ID 381243); published 10 December 2019

We demonstrate a nanosecond pulsed source at 620 nm with watt-level average power by frequency-doubling a 1240 nm phosphosilicate Raman fiber amplifier. A gain-switched laser diode operating at 1064 nm is amplified in an ytterbium fiber master oscillator power amplifier system and then converted to 1240 nm using a phosphosilicate Raman fiber amplifier with a conversion efficiency of up to 66%. The Raman fiber amplifier is seeded with a continuous-wave 1240 nm laser diode to obtain narrow-linewidth radiation, which is subsequently frequency-doubled in a periodically poled lithium tantalate crystal. A maximum average power of 1.5 W is generated at 620 nm, corresponding to a pulse energy of 300 nJ at a repetition rate of 5 MHz. The source has excellent beam quality ($M^2 \leq 1.16$) and an optical efficiency (1064 nm to 620 nm) of 20%, demonstrating an effective architecture for generating red pulsed light for biomedical imaging applications.

https://doi.org/10.1364/OL.44.006025

Nanosecond pulsed sources in the red spectral region are required for applications including stimulated emission depletion (STED) microscopy [1], and optical-resolution photoacoustic microscopy (OR-PAM) [2]. In particular, for STED microscopy, the enhancement in imaging resolution scales with the pulse energy of the beam used for depletion, making sources with hundreds of nanojoules of pulse energy desirable [3]. Using a red laser for depletion allows for increased penetration depth and reduced photodamage in biological tissue as compared to green lasers [4]. Depletion is most efficient with pulse durations between 0.1 ns and 2 ns, with repetition rates of several MHz being favored to avoid photobleaching while maintaining fast image acquisition times [5].

There are limited pulsed red sources that satisfy these requirements. Supercontinuum sources must be spectrally filtered, resulting in poor overall optical efficiencies and low pulse energies from commercially available systems [5]. Laser diodes have limited pulse energy in single transverse spatial mode configurations and are not available between 525 nm and 630 nm. Ultrafast optical parametric oscillators are capable of providing the necessary operating parameters [6], but they have fixed repetition rates, are expensive, and have large footprints.

Pulsed ytterbium-fiber (Yb:fiber) master oscillator power amplifier (MOPA) systems can be frequency-doubled to implement practical, high-energy green sources between 515 nm and 550 nm with near-diffraction-limited beam quality [7]. However, operating high-gain Yb:fiber MOPA systems beyond 1100 nm is challenging due to the larger emission cross section at shorter wavelengths, leading to issues with amplified spontaneous emission around 1030 nm [8]. Bismuth-doped aluminosilicate fibers exhibit broadband luminescence in the 1150–1300 nm region but have insufficient gain >1200 nm to implement pulsed MOPA systems [9]. To access the red spectral region, praseodymium-doped fluoride fiber MOPA systems have been frequency-doubled [10], but power scaling is limited and wavelengths less than 640 nm cannot be generated [11].

Stimulated Raman scattering (SRS) in optical fibers can be harnessed to provide gain outside the emission bands of rare-earth-doped fibers. The combination of SRS followed by second-harmonic generation (SHG) is a highly efficient and practical method for accessing the yellow-green spectral region using readily available Yb:fiber MOPA systems [12]. However, accessing the red spectral region via SRS and subsequent SHG would require at least three Stokes shifts in silica fibers, since they have a Raman gain peak at a frequency downshift of ∼13 THz. Multiple Stokes shifts reduce the overall optical efficiency and broaden the spectral bandwidth of the generated light due to competing nonlinear processes. This can reduce the subsequent SHG conversion efficiency due to the finite spectral acceptance bandwidth of SHG crystals [7].

In phosphosilicate fibers, in addition to the ∼13 THz Raman gain peak of silica fibers, there is a peak at a frequency downshift of 40 THz due to stretching vibrations of oxygen–phosphorous double bonds [13]. This enables the red spectral region to be accessed via SHG after only a single Stokes shift from 1064 nm to 1240 nm using an Yb:fiber MOPA system. To date, this has only been demonstrated using frequency-doubled continuous-wave (CW) phosphosilicate Raman fiber lasers [14,15]. In this Letter, we report a new architecture for

efficiently generating nanosecond pulsed light at 620 nm, by frequency-doubling a pulsed phosphosilicate Raman fiber amplifier. The system generated a maximum 620 nm average power of 1.5 W, corresponding to a pulse energy of 300 nJ at a repetition rate of 5 MHz with a pulse duration of 1 ns.

A pulsed Yb:fiber MOPA system operating at 1064 nm was converted to 1240 nm in a phosphosilicate Raman fiber amplifier, seeded by a narrow-linewidth CW laser diode at 1240 nm. The generated 1240 nm light adopts the temporal properties of the Yb:fiber MOPA system, as the Raman gain is available only in the window of the 1064 nm pulses [12]. Using a 1240 nm seed diode operating CW avoids the need for any synchronization electronics with the Yb:fiber MOPA pulses. The 1240 nm light was subsequently frequency-doubled in a periodically poled stoichiometric lithium tantalate (PPLT) crystal. The source had near-diffraction-limited beam quality ($M^2 \leq 1.16$), subnanometer spectral linewidth ($\leq$100 pm), and ideal parameters for biophotonics imaging applications such as STED microscopy and OR-PAM. This is, to the best of our knowledge, the first demonstration of a frequency-doubled phosphosilicate Raman fiber amplifier.

A 1064 nm gain-switched laser diode (QDLaser) provided pulses of 1.2 ns duration at a repetition rate of 5 MHz, with a pulse energy of 64 pJ. These pulses were amplified to a pulse energy of 900 pJ in a polarization-maintaining (PM) Yb:fiber pre-amplifier, and then to 1.5 μJ in a PM Yb:fiber power-amplifier (IPG Photonics) [Fig. 1]. The temporal profile of the laser diode output pulses and power amplifier pulses can be seen in Figs. 2(a) and 2(b), respectively. The relaxation oscillation at the leading edge of the diode pulse, 50 ps in duration, is characteristic of the pulse dynamics in gain-switched laser diodes [16].

A 5 m length of PM phosphosilicate fiber (FORC P-SM-5-PM, PM P-fiber Fig. 1) was used as the Raman fiber amplifier gain medium. The length of phosphosilicate fiber used, in conjunction with the chosen 1064 nm input peak power, must be carefully chosen to minimize deleterious nonlinear effects and the onset of other Raman Stokes shifts while maintaining a high level of conversion to 1240 nm. These Stokes lines include those at 1120 nm and 1310 nm due to the 13 THz Raman shift, and at 1480 nm, due to the 40 THz Raman shift.

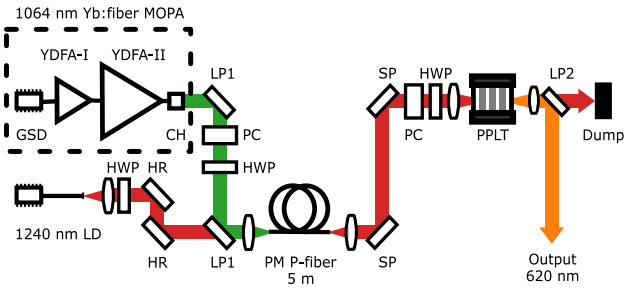

Fig. 1. 1240 nm phosphosilicate Raman fiber amplifier and subsequent frequency doubling in a periodically poled lithium tantalate crystal. GSD, gain-switched laser diode; YDFA-I, Yb-doped fiber pre-amplifier; YDFA-II, Yb-doped fiber power amplifier; CH, collimator head; LD, laser diode; P-fiber, phosphosilicate fiber; HWP, half-wave plate; PC, power control, formed of half-wave plate and polarizing beam splitter cube; HR, highly reflective mirror at 1240 nm; LP1, longpass filter (cut-on 1150 nm); LP2, longpass filter (cut-on 900 nm); SP, shortpass filter (cutoff 1100 nm).

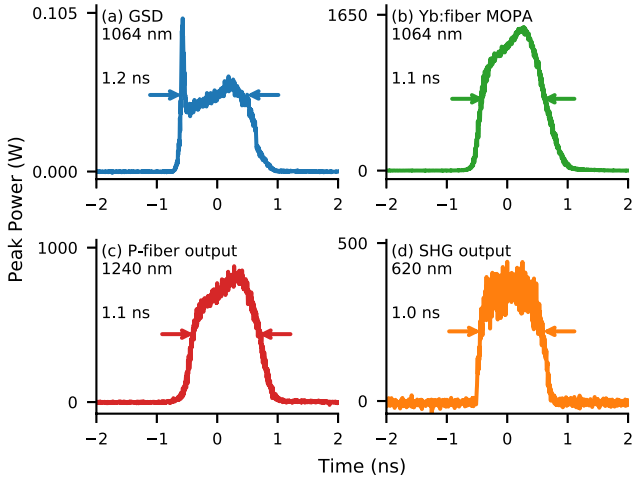

Fig. 2. Temporal profiles of the output pulses of the (a) 1064 nm gain-switched laser diode (GSD), (b) Yb:fiber MOPA, (c) phosphosilicate fiber (P-fiber) amplifier, and (d) 620 nm SHG output from the PPLT crystal. The full-width-half-maximum (FWHM) pulse duration is indicated in each case.

A fiber Bragg grating stabilized laser diode operating at 1240 nm (Innolume) was used to provide a CW, linearly polarized seed signal to the Raman amplifier. The diode provided up to 300 mW of power at 1240 nm, with a 3 dB spectral linewidth of 20 pm. A maximum of 200 mW of 1240 nm light was coupled into the phosphosilicate fiber. The 1064 nm pump and 1240 nm seed beams were combined using a pair of longpass filters with a cut-on at 1150 nm (Thorlabs DMLP1150). The use of PM components throughout the system ensured that both the 1064 nm Yb:fiber amplifier output pulses and 1240 nm seed light were linearly polarized and coupled onto one of the principal axes of the phosphosilicate Raman fiber, to maximize the Raman gain.

Figure 3(a) shows that the average power at 1240 nm generated within a bandwidth of 40 nm, sufficient to incorporate the entire spectral feature at 1240 nm, increases monotonically with 1064 nm input power (orange points). However, the average 1240 nm power generated within a smaller bandwidth of 0.24 nm (the spectral acceptance bandwidth of the PPLT crystal, discussed later) begins to roll-off at 1064 nm input powers of greater than 8 W (blue points). The 3 dB spectral linewidth of the amplified 1240 nm signal was 20 pm for all amplifier output powers up to 12 W. This was the same as the 3 dB linewidth of the 1240 nm seed diode, showing that there was no spectral broadening of the linewidth due to nonlinear effects such as self-phase modulation. The roll-off in power was instead due to the growth of a pedestal around the 1240 nm signal. Any power outside the 0.24 nm spectral acceptance bandwidth of the PPLT crystal will decrease the SHG conversion efficiency. Thus, the Raman amplifier was operated at a power of 7.5 W for the frequency doubling.

Figure 3(b) shows the generated average power at 1240 nm (orange points) and the corresponding amplifier gain (blue points) as a function of 1240 nm seed power for a 1064 nm input power of 8 W. Above a seed power of 1 mW, there was a sharp roll-off in the generated 1240 nm power, and the amplifier gain strongly saturated with increasing seed power. The amplifier gain was calculated using the effective seed power, rather

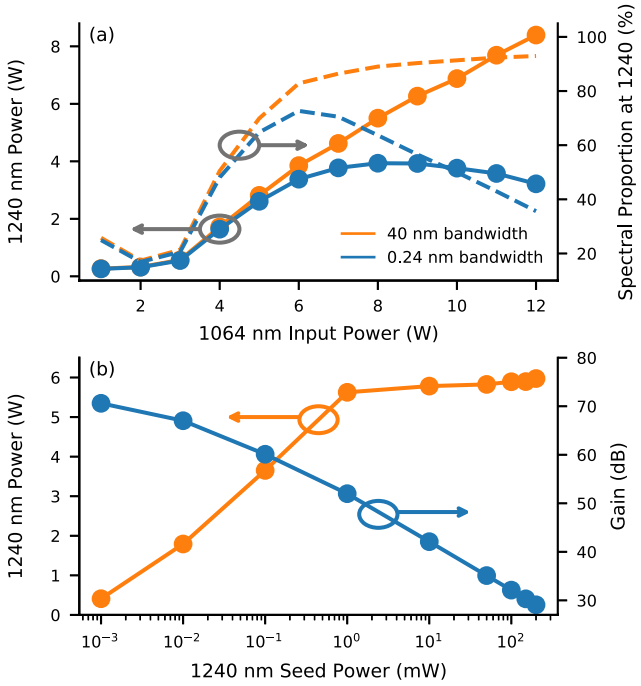

Fig. 3. (a) Calculated phosphosilicate Raman fiber amplifier output power (points) and percentage spectral content (dashed lines) as a function of input 1064 nm power for a 40 nm (orange) and 0.24 nm (blue) integration bandwidth at 1240 nm. (b) Generated 1240 nm power (orange) and phosphosilicate Raman fiber amplifier gain (blue) as a function of seed power, for an Yb:fiber MOPA power of 8 W.

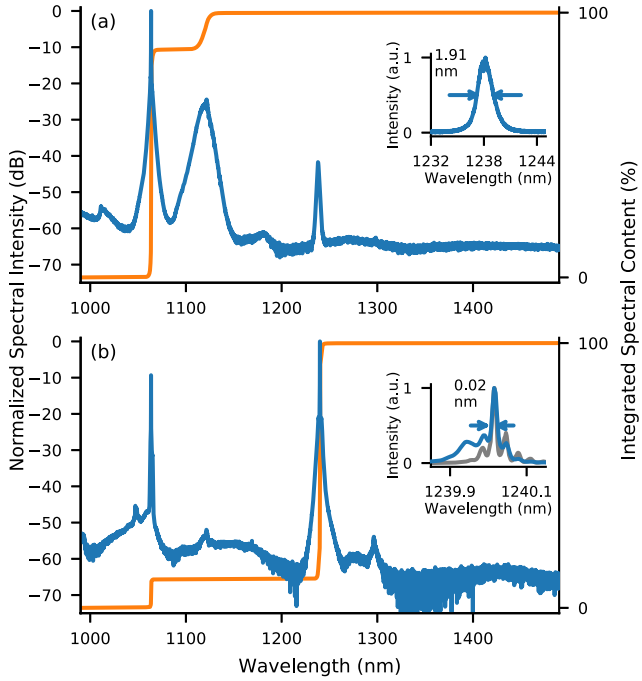

Fig. 4. Spectra of the phosphosilicate Raman fiber amplifier output for a 1064 nm input power of 8 W where (a) no seed light is present and (b) 200 mW of seed power are coupled into the phosphosilicate fiber. The orange lines show the integrated spectral content as a function of wavelength. Insets show optical spectrum of the generated 1240 nm light (blue) and 1240 nm seed diode (gray) on a linear scale.

than the total 1240 nm seed power coupled into the phosphosilicate fiber. This effective seed power was the total 1240 nm seed power divided by the duty cycle of the Yb:fiber MOPA system, since the Raman gain is negligible outside the pump pulses.

Figure 4(a) shows the optical spectrum of the phosphosilicate Raman fiber amplifier output at a 1064 nm input power of 8 W in the case where no seed light is present, as well as the integrated spectral content as a function of wavelength. In the unseeded case, only 0.07% of the output spectral content was contained within a 40 nm bandwidth centered at 1240 nm. The majority of the spectral content instead comprised the residual 1064 nm input power and light at the first 13 THz Raman Stokes shift at 1120 nm. Moreover, the linewidth of the generated 1240 nm was broad, with a 3 dB spectral bandwidth of 1.91 nm. In contrast, Fig. 4(b) shows the optical spectrum of the phosphosilicate Raman fiber amplifier output for 8 W of 1064 nm input power and 200 mW of coupled 1240 nm seed power. In this case, 89% of the light was contained within a 40 nm bandwidth centered at 1240 nm.

The Raman fiber amplifier was highly efficient; the conversion efficiency from 1064 nm input power to 1240 nm output power was 66% at a 1064 nm input power of 8 W. Accounting for coupling losses, the internal conversion efficiency of 1064 nm to 1240 nm in the Raman fiber amplifier was 79%, close to the maximum quantum defect limited conversion efficiency of 85%.

The temporal profile of the generated 1240 nm pulses can be seen in Fig. 2(c). The pulses have a full-width-half-maximum (FWHM) duration of 1.1 ns and follow the temporal profile of the 1064 nm pump pulses [Fig. 2(b)]. The phosphosilicate fiber used has a cutoff wavelength of <1060 nm and is therefore single mode for both the pump and signal wavelengths. The beam quality of the amplified 1240 nm signal was measured to be $M^2 = 1.01$ using a pyroelectric scanning slit beam profiler.

The high-power spectral density, linearly polarized 1240 nm output of the phosphosilicate Raman fiber amplifier had ideal parameters for efficient SHG using a periodically poled crystal. A 20 mm long, AR-coated, periodically poled stoichiometric lithium tantalate (PPLT) crystal (Deltronic) with a 0.5×10 mm^2 aperture, containing multiple gratings, was used for frequency doubling. A grating with a poling period of 12.1 μm was used for quasi-phase-matching SHG of 1240 nm at a crystal temperature of ~140°C. Using the Sellmeier equation of Dolev *et al.* [17], the 3 dB spectral acceptance bandwidth of this interaction was calculated to be 0.24 nm in the low pump depletion regime.

The output of the phosphosilicate Raman fiber amplifier was filtered using a pair of shortpass dichroic mirrors with a cutoff at 1100 nm (Edmund Optics) to remove the residual 1064 nm light. A half-wave plate and polarizing beam splitter cube were used to control the power incident on the crystal (power control, Fig. 1). A second half-wave plate was used to align the polarization axis of the 1240 nm light to the z axis of the PPLT crystal to utilize type-0 (all waves extraordinarily polarized) phase matching.

The 1240 nm beam was focused into the PPLT crystal using an AR-coated, $f = 63$ mm plano-convex lens. The focused $1/e^2$ beam diameter in air was measured to be 70 μm using a pyroelectric scanning slit beam profiler. This corresponds to a focusing parameter of $\xi = L/b = 1.6$, where L is the crystal

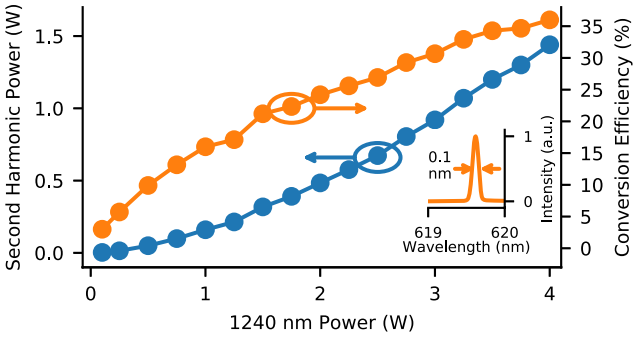

Fig. 5. Second-harmonic average power at 620 nm (blue points) and conversion efficiency (orange points) as a function of the 1240 nm power into the PPLT crystal. Lines are a guide for the eye. Inset shows the optical spectrum of the generated 620 nm light on a linear scale.

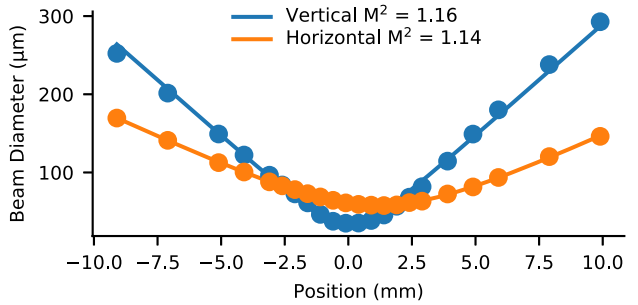

Fig. 6. Beam quality measurement at 1.5 W of 620 nm power with a Gaussian fit (lines) to the measured beam diameters (points) through the focus of an f = 100 mm plano-convex lens.

length and b is the confocal parameter of the 1240 nm beam in the crystal [18]. The estimated peak intensity of the 1240 nm beam in the crystal was ~45 MW/cm^2. The 1240 nm pulse peak power was calculated by equating the integrated pulse profile with the pulse energy.

Figure 5 shows the generated 620 nm average power as a function of the 1240 nm pump power. A maximum 620 nm average power of 1.5 W was generated for a 1240 nm pump power of 4.0 W, corresponding to a conversion efficiency of 38%. There is no roll-off in the SHG conversion efficiency (orange points Fig. 5), suggesting that higher conversion efficiencies could be achieved with greater peak power at 1240 nm. The 3 dB spectral bandwidth of the 620 nm light was ≤ 0.1 nm, limited by the resolution of the optical spectrum analyzer (inset Fig. 5).

The 620 nm pulses [Fig. 2(d)] had a FWHM duration of 1.0 ns, which was shortened from the 1240 nm pulses [Fig. 2(c)] due to the nonlinear relationship between the SHG conversion efficiency and the instantaneous power of the pump pulse. This pulse duration is well suited to OR-PAM and STED microscopy [2,5]. The 620 nm beam quality was measured at an average power of 1.5 W using a pyroelectric scanning slit beam profiler to measure the 4σ beam diameter through the focus of an f = 100 mm plano-convex lens. Figure 6 shows the measured beam diameter (points) with a Gaussian fit to the beam caustics (lines), which revealed an $M^2 = 1.16$ and $M^2 = 1.14$ in the vertical and horizontal axes, respectively.

We have demonstrated a new architecture for generating MHz repetition rate, nanosecond pulsed light at 620 nm using a phosphosilicate fiber to provide Raman gain. By seeding the phosphosilicate Raman fiber amplifier with a 1240 nm CW signal, conversion from 1064 nm pump pulses to narrow bandwidth 1240 nm pulses exceeded 66% (79% when accounting for coupling losses). The output of the phosphosilicate Raman amplifier was frequency-doubled, generating a maximum average power of 1.5 W at 620 nm, corresponding to a conversion efficiency of 38%. The generated 620 nm light had a pulse duration of 1 ns and a repetition rate of 5 MHz, with a pulse energy of 300 nJ, ideal parameters for STED microscopy and OR-PAM. This technique is flexible in repetition rate and pulse duration [19], and can be fully fiber integrated. This architecture can be used to generate light between 595-640 nm, by varying the Yb:fiber MOPA and seed diode wavelengths. Our new, single Raman shift architecture provides a simple way of generating nanosecond-pulsed sources in the orange and red spectral regions.

Funding. Engineering and Physical Sciences Research Council (EP/N009452/1, EP/R511547/1); Medical Research Council (MR/K015834/1); The European Office of Aerospace Research and Development (FA9550-17-1-0194).

Acknowledgment. The data used in this paper are openly available at: https://doi.org/10.5281/zenodo.3532834.

REFERENCES

1. B. R. Rankin and S. W. Hell, Opt. Express **17**, 15679 (2009).
2. J. Yao, K. I. Maslov, S. Hu, and L. V. Wang, J. Biomed. Opt. **14**, 054049 (2009).
3. S. W. Hell and J. Wichmann, Opt. Lett. **19**, 780 (1994).
4. W. Wegner, P. Ilgen, C. Gregor, J. V. Dort, A. C. Mott, H. Steffens, and K. I. Willig, Sci. Rep. **7**, 11781 (2017).
5. D. Wildanger, E. Rittweger, L. Kastrup, and S. W. Hell, Opt. Express **16**, 9614 (2008).
6. M. A. Lauterbach, M. Guillon, A. Soltani, and V. Emiliani, Sci. Rep. **3**, 2050 (2013).
7. A. Avdokhin, V. Gapontsev, P. Kadwani, A. Vaupel, I. Samartsev, N. Platonov, A. Yusim, and D. Myasnikov, Proc. SPIE **9347**, 934704 (2015).
8. J. He, D. Lin, L. Xu, M. Beresna, M. N. Zervas, S. Alam, and G. Brambilla, IEEE Photon. Technol. Lett. **31**, 727 (2019).
9. I. Bufetov and E. Dianov, Laser Phys. Lett. **6**, 487 (2009).
10. J.-H. Hung, K. Sato, Y.-C. Fang, L.-H. Peng, T. Nemoto, and H. Yokoyama, Appl. Phys. Express **10**, 102701 (2017).
11. T. J. Whitley, J. Lightwave Technol. **13**, 744 (1995).
12. T. H. Runcorn, F. G. Görlitz, R. T. Murray, and E. J. R. Kelleher, IEEE J. Sel. Top. Quantum Electron. **24**, 1 (2018).
13. E. M. Dianov, M. V. Grekov, I. A. Bufetov, S. A. Vasiliev, O. I. Medvedkov, V. G. Plotnichenko, V. V. Koltashev, A. V. Belov, M. M. Bubnov, S. L. Semjonov, and A. M. Prokhorov, Electron. Lett. **33**, 1542 (1997).
14. S. I. Kablukov, S. A. Babin, D. V. Churkin, A. V. Denisov, and D. S. Kharenko, Opt. Express **17**, 5980 (2009).
15. A. A. Surin, S. V. Larin, T. Borisenko, K. Y. Prusakov, and Y. S. Stirmanov, Quantum Electron. **46**, 1097 (2016).
16. S. M. Riecke, H. Wenzel, S. Schwertfeger, K. Lauritsen, K. Paschke, R. Erdmann, and G. Erbert, IEEE J. Quantum Electron. **47**, 715 (2011).
17. I. Dolev, A. Ganany-Padowicz, O. Gayer, A. Arie, J. Mangin, and G. Gadret, Appl. Phys. B **96**, 423 (2009).
18. D. A. Kleinman, A. Ashkin, and G. D. Boyd, Phys. Rev. **145**, 338 (1966).
19. T. H. Runcorn, R. T. Murray, E. J. R. Kelleher, S. V. Popov, and J. R. Taylor, Opt. Lett. **40**, 3085 (2015).